Lanthanide Chelates Containing Pyridine Units with Potential Application as Contrast Agents in Magnetic Resonance Imaging

Carlos Platas-Iglesias,*[a] Marta Mato-Iglesias,[a] Kristina Djanashvili,[b] Robert N. Muller,[c] Luce Vander Elst,[c] Joop A. Peters,[b] Andrés de Blas,*[a] and Teresa Rodríguez-Blas[a]

Abstract: A new pyridine-containing ligand, *N*,*N*′-bis(6-carboxy-2-pyridylmethyl)ethylenediamine-*N*,*N*′-diacetic acid (H_4L), has been designed for the complexation of lanthanide ions. ^1H and ^{13}C NMR studies in D_2O solutions show octadentate binding of the ligand to the Ln^{III} ions through the nitrogen atoms of two amine groups, the oxygen atoms of four carboxylates, and the two nitrogen atoms of the pyridine rings. Luminescence measurements demonstrate that both Eu^{III} and Tb^{III} complexes are nine-coordinate, whereby a water molecule completes the Ln^{III} coordination sphere. Ligand L can sensitize both the Eu^{III} and Tb^{III} luminescence; however, the quantum yields of the Eu^{III}- and Tb^{III}-centered luminescence remain modest. This is explained in terms of energy differences between the singlet and triplet states on the one hand, and between the 0-phonon transition of the triplet state and the excited metal ion states on the other. The anionic $[Ln(L)(H_2O)]^-$ complexes (Ln = La, Pr, and Gd) were also characterized by theoretical calculations both in vacuo and in aqueous solution (PCM model) at the HF level by means of the 3–21G* basis set for the ligand atoms and a $46+4f^n$ effective core potential for the lanthanides. The structures obtained from these theoretical calculations are in very good agreement with the experimental solution structures, as demonstrated by paramagnetic NMR measurements (lanthanide-induced shifts and relaxation-rate enhancements). Data sets obtained from variable-temperature ^{17}O NMR at 7.05 T and variable-temperature ^1H nuclear magnetic relaxation dispersion (NMRD) on the Gd^{III} complex were fitted simultaneously to give insight into the parameters that govern the water ^1H relaxivity. The water exchange rate ($k_{ex}^{298} = 5.0 \times 10^6\ s^{-1}$) is slightly faster than in $[Gd(dota)(H_2O)]^-$ (DOTA = 1,4,7,10-tetrakis(carboxymethyl)-1,4,7,10-tetraazacyclododecane). Fast rotation limits the relaxivity under the usual MRI conditions.

Keywords: chelates · contrast agents · gadolinium · lanthanides · magnetic resonance imaging

Introduction

Lanthanide coordination compounds[1] are the subject of intense research efforts owing to their applications as contrast agents for magnetic resonance imaging (MRI),[2,3] as catalysts in RNA hydrolysis,[4] as responsive luminescent lanthanide complexes,[5] or as active agents in cancer radiotherapy.[6] In particular, gadolinium complexes with poly(aminocarboxylate) ligands, such as $[Gd(dtpa)(H_2O)]^{2-}$ (DTPA = diethylenetriamine-*N*,*N*,*N*′,*N*″,*N*″-pentaacetate), [Gd(dtpa-bma)(H_2O)] (DTPA-BMA = DTPA-bis(methylamide), $[Gd(dota)(H_2O)]^-$ (DOTA = 1,4,7,10-tetraazacyclododecane-1,4,7,10-tetraacetate), and [Gd(hp-do3a)(H_2O)] (HP-DO3A = 10-(2-hydroxypropyl)-1,4,7,10-tetraazacyclododecane-1,4,7-triacetate), attract considerable interest since they are commonly used as contrast agents in MRI.[2,3] Currently, approximately one third of all MRI scans are made after administration of a Gd^{III}-based contrast agent.[3] Contrast agents enhance the image contrast by preferentially in-

[a] Dr. C. Platas-Iglesias, M. Mato-Iglesias, Dr. A. de Blas, Dr. T. Rodríguez-Blas
Dpto. Química Fundamental, Facultade de Ciencias
Campus da Zapateira s/n, Universidade da Coruña
15071 A Coruña (Spain)
Fax(+34) 981-167065
E-mail: mayter@udc.es

[b] K. Djanashvili, Dr. J. A. Peters
Laboratory of Applied Organic Chemistry and Catalysis
Delft University of Technology
Julianalaan 136, 2628 BL Delft (The Netherlands)

[c] Dr. R. N. Muller, Dr. L. V. Elst
NMR Laboratory, Department of Organic Chemistry
University of Mons-Hainaut
7000 Mons (Belgium)

Supporting information for this article is available on the WWW under http://www.chemeurj.org/ or from the author.

 DOI: 10.1002/chem.200306031

fluencing the relaxation efficiency of the water proton nuclei in the target tissue. The efficiency of a contrast agent is evaluated in terms of its relaxivity, which is defined as the relaxation-rate enhancement of water proton nuclei per mM concentration of metal ion. These complexes contain at least one Gd^{III}-bound water molecule that rapidly exchanges with the bulk water of the body; this imparts an efficient mechanism for the longitudinal and transverse relaxation (T_1 and T_2) enhancement of water protons. Around a paramagnetic ion, the relaxation rates of the bulk water proton are enhanced as a result of long-range interactions (outer-sphere relaxation) and short-range interactions (inner-sphere relaxation). According to the standard Solomon–Bloembergen–Morgan model, the latter process is governed by four correlation times: the rotational correlation time of the complex (τ_R), the residence time of a water proton in the inner coordination sphere (τ_m), and the electronic longitudinal and transverse relaxation rates ($1/T_{1e}$ and $1/T_{2e}$) of the metal center.[7]

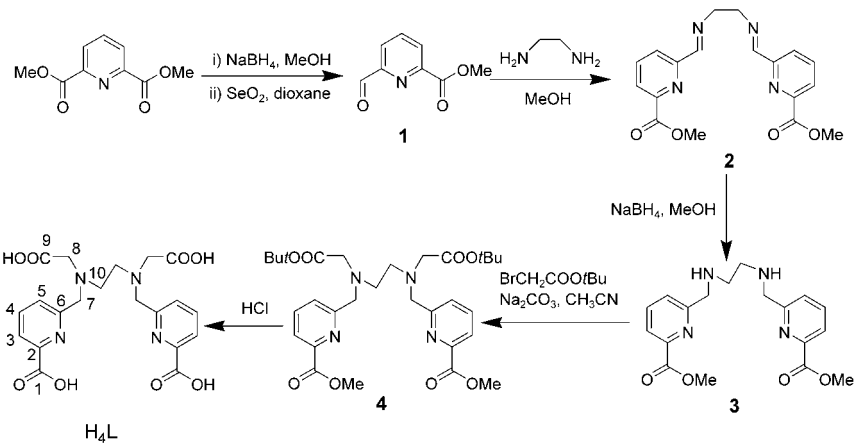

Scheme 1. Synthesis protocol for the ligand used in this work.

The theory predicts that high relaxivities at the imaging fields (0.5–1.5 T) may be observed for systems with a long rotational correlation time and relatively fast water exchange.[7] Several approaches have been used to increase the τ_R values of paramagnetic complexes, including covalent binding to slowly tumbling substrates, such as dextran[8] or inulin,[9] formation of self-aggregates in solution,[10,11] or formation of noncovalent adducts with β-cyclodextrin[12] or albumin.[13] The latter approach requires the design of Gd^{III} chelates, such as MS-325[14] that bear suitable functionalities on their surface that promote the reversible binding of albumin. Besides the attainment of high relaxivities, the approach developed for binding albumin has been extended to other proteins, which allows the preparation of new contrast agents designed to recognize a target of interest.[15]

In the search for new Gd^{III} chelates that could be further functionalized with groups able to target biological material for application as contrast agents in MRI, we report here on investigation of the new ligand H_4L (Scheme 1). This ligand is potentially octadentate for the coordination of Ln^{III} ions and contains pyridine units that can be easily functionalized with groups able to conjugate with biological material.[16,17] The corresponding lanthanide complexes were characterized by ^1H and ^{13}C NMR techniques in D_2O solution. Luminescence studies have been carried out to test the ability of the ligand to promote a good antenna effect for Eu^{III} and Tb^{III}, as well as to determine the hydration number of the complexes in solution. The complexes were also characterized by ab initio calculations both in vacuo and in aqueous solution (PCM model). The structures obtained from these calculations were compared with the structural information obtained in solution from paramagnetic NMR measurements (lanthanide-induced shifts and relaxation-rate enhancements). Finally, nuclear magnetic resonance dispersion (NMRD) investigations and variable-temperature ^{17}O NMR measurements of the complex formed with Gd^{III} were conducted in order to assess its ^1H relaxation enhancement abilities in water and to gain insight into the parameters that govern this relaxation process.

Results and Discussion

Syntheses of the ligand: *N*,*N*′-Bis(6-carboxy-2-pyridylmethyl)ethylenediamine-*N*,*N*′-diacetic acid (H_4L) was obtained in five steps from dimethyl pyridine-2,6-dicarboxylate by means of the procedure described in the Experimental Section (Scheme 1). Methoxypyridine aldehyde (**1**) was obtained in good yield (70%) by partial reduction of the latter with sodium tetrahydroborate followed by oxidation with SeO_2. Aldehyde **1** was treated with ethylenediamine to give the Schiff base **2** (80%), which was reduced with sodium tetrahydroborate to afford amine **3** in 85% yield. Attempts to alkylate **3** with ethyl bromoacetate in refluxing CH_3CN in the presence of Na_2CO_3 yielded intractable mixtures, probably as a result of the formation of lactams and intermolecular side products, in addition to the target compound.[18] However, alkylation of **3** with *tert*-butyl bromoacetate under similar conditions gave compound **4** in 26% yield. Reaction of **4** with trifluoroacetic acid at room temperature resulted in the selective deprotection of the *tert*-butyl esters. Full deprotection of methyl and *tert*-butyl esters in **4** was cleanly achieved with 6M HCl to yield the desired ligand H_4L.

^1H and ^{13}C NMR spectra: The ^1H and ^{13}C NMR spectra of the La^{III} complex of L were obtained in D_2O at pD = 7.0. The proton spectrum (Figure 1) consists of nine signals corresponding to the nine different proton magnetic environments of the ligand molecule (see Scheme 1 for labeling). This points to an effective C_2 symmetry of the complexes in solution that is confirmed by the ^{13}C spectrum, which shows ten NMR peaks for the 20 carbon nuclei of the ligand back-

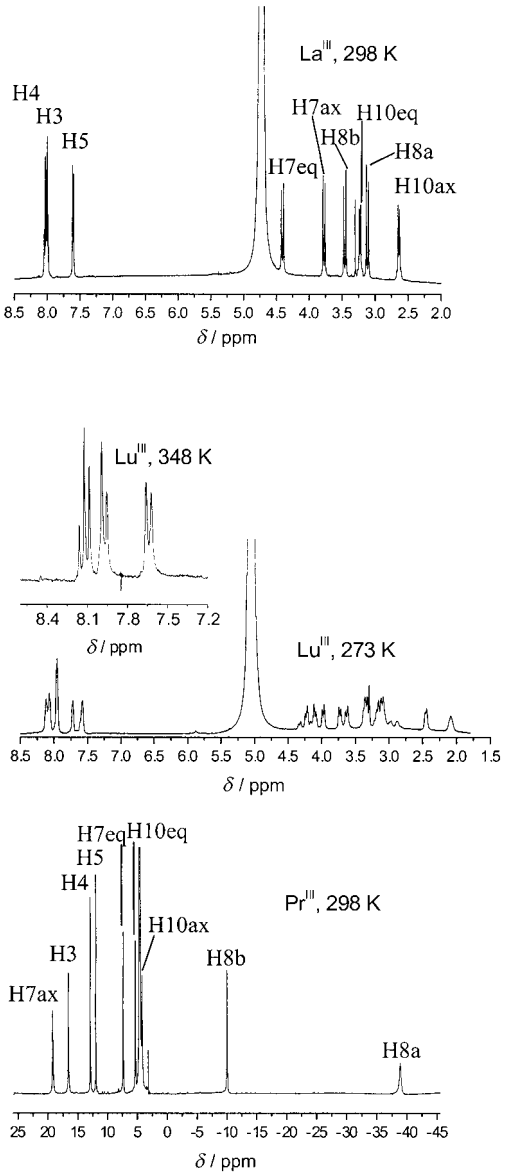

Figure 1. ^{1}H NMR (500 MHz) spectra of the ligand complexes in D_2O (30 mM, pH 7.0).

bone. The assignments of the proton signals (Table 1) were based upon shift comparisons with other polyazacarboxylate lanthanum complexes,[19] and standard 2D homonuclear COSY experiments, which gave strong crosspeaks between the geminal CH_2 protons (7, 8, and 10) and between *ortho*-coupled pyridyl protons.

A full assignment of the ^{1}H and ^{13}C NMR spectra was achieved with the aid of HMQC and HMBC 2D heteronuclear experiments. Although the specific CH_2 proton assignments H10ax/H10eq, H8a/H8b, and H7ax/H7eq, were not possible on the basis of the 2D NMR spectra, they were successfully assigned by means of the stereochemically dependent proton-shift effects that result from the polarization of the C–H bonds by the electric-field effect caused by the cation charge.[20] This results in a deshielding effect of the H10eq, H7eq, and H8b protons, which are pointing away from the La^{III} ion. The bridging methylene protons CH_2(7ax) and CH_2(7eq) show an AB pattern at $\delta = 3.65$ and 4.28 ppm, respectively, whereby the larger shift for CH_2(7eq) probably results from the combined deshielding effects of the pyridyl ring current and polarizing effect of La^{III} on the C–H_{eq} bond pointing away from it.

The ^{1}H NMR spectrum of the diamagnetic Lu^{III} complex recorded at 273 K is much more complex than that of La^{III}. At this temperature, the spectrum of the Lu^{III} complex corresponds to a species with an effective C_1 symmetry in solution (Figure 1). Increasing the temperature results in a substantial increase of the linewidths, reflecting intramolecular conformational exchange processes. In spite of the increasing complexity of the spectra on increasing the temperature, especially in the region in which the aliphatic proton signals occur, some temperature-dependent spectral changes can be analyzed and interpreted. At 273 K, the ^{1}H NMR spectrum shows a pair of signals with equal intensity for each of the H3, H4, and H5 protons (Figure 1). The linewidths of these signals gradually increase above this temperature, and a much simpler spectrum consisting of one triplet and two doublet signals is obtained at 348 K (Figure 1). This is in agreement with an effective C_2 symmetry of the complex in solution at this temperature. If it is assumed that the exchange process associated with this line broadening (before coalescence) is slow on the NMR timescale, then the exchange rate for this dynamic process (k) can be calculated from the observed linewidths at half-height ($\Delta\nu_{1/2}$) [Eq. (1)]:

$$k = \pi(\Delta\nu_{1/2} - \Delta\nu_{1/2}(0)) \quad (1)$$

in which $\Delta\nu_{1/2}(0)$ is the linewidth in absence of exchange. A plot of $\ln(k/T)$ versus $1/T$ [$k = (k_b T/h)\exp(\Delta S^{+}/R - \Delta H^{+}/RT)$] (in which k_b and h are the Boltzmann and Planck constants respectively, T is the absolute temperature, and k is the rate constant) yields the activation parameters for the

Table 1. ^{1}H NMR shifts [500 MHz, ppm], computed values for contact (F_i) and dipolar (G_i) terms, as well as agreement factors (AF_i) for solutions of $[Ln(L)(H_2O)]^-$ complexes in D_2O (30 mM) at pH 7.0

	H3	H4	H5	H7ax	H7eq	H8a	H8b	H10ax	H10eq
La[a]	7.99	8.03	7.60	3.77	4.41	3.12	3.46	2.64	3.23
Ce[b]	12.10	9.98	8.52	12.59	3.02	−26.24	−6.82	4.90	2.78
Pr[b]	16.61	12.95	12.03	19.23	7.42	−38.85	−9.99	4.23	5.40
Nd	14.13	11.97	10.86	12.91	10.01	−18.89	−2.54	2.34	6.98
Sm	8.63	8.25	7.64	6.76	3.41	-2.72	1.07	4.25	2.58
F_i	−0.3(3)	0.2(2)	0.5(3)	−5.3(9)	2.8(3)	8.10(2)	4.09(6)	−3.8(4)	1.88(8)
G_i	0.76(8)	0.32(5)	0.14(9)	2.4(3)	−0.60(8)	−5.8874(8)	−2.29(1)	1.0(1)	−0.34(2)
AF_i[c]	0.0161	0.0259	0.107	0.0184	0.164	0.00051	0.00059	0.579	0.163

[a] Assignment supported by 2D H,H-COSY, HMQC, and HMBC experiments at 298 K. ^2J(10ax,10eq) = 10.9 Hz, ^2J(10eq,10ax) = 10.6 Hz, $^2J(8_b,8_a) = 16.2$ Hz, $^2J(8_a,8_b) = 16.5$ Hz, ^2J(7eq,7ax) = 15.3 Hz, ^2J(7ax,7eq) = 15.3 Hz, ^3J(5,4) = 7.2 Hz, ^3J(3,4) = 7.5 Hz. [b] Assignment supported by 2D H,H-COSY experiments at 298 K. [c] Agreement factors calculated according to Equation (6); F_i and G_i were calculated with the data obtained for the Ce^{III}, Pr^{III}, and Sm^{III} complexes only (see text).

interconversion process ($\Delta G^{\neq} = 36 \pm 2$ kJ mol^{-1}, $\Delta H^{\neq} = 15.9 \pm 0.8$ kJ mol^{-1}, $\Delta S^{\neq} = -68 \pm 3$ J mol^{-1} K^{-1}, $k = 3.0 \times 10^6 \pm 1.4 \times 10^6$ s^{-1}). This activation barrier is relatively low. Much higher activation barriers were determined for dynamic processes that require partial decoordination of the ligand in poly(aminocarboxylate) complexes.[21,22] This indicates that the intramolecular dynamic behavior observed for the Lu^{III} complex of the ligand does not require a partial decoordination of the ligand. Our ab initio calculations (vide infra) show that the presence of a coordinated water molecule in the complexes results in distorted C_2 symmetries. These results suggest that the intramolecular dynamic behavior observed for the Lu^{III} complex of the ligand corresponds to small adjustments of the Lu^{III} coordination sphere that are fast on the NMR timescale at high temperatures, leading to an effective C_2 symmetry in solution.

^{1}H NMR spectra of the paramagnetic Ce, Pr, Nd, and Sm complexes were obtained in D_2O at pD = 7.0. The spectrum of the Pr^{III} complex is shown in Figure 1. The spectrum of the Sm^{III} complex displays relatively small paramagnetic shifts, and the signals were assigned by a simple comparison with the spectrum of the diamagnetic La^{III} complex. The spectra of the Ce^{III} and Pr^{III} complexes were assigned with the aid of a linewidth analysis and COSY spectra, which gave crosspeaks between the geminal CH_2 protons and between *ortho*-pyridyl protons. A full assignment of the spectra was supported by the experimental LIS values according to Equations (4) and (5) (vide infra), allowing for permutations of two selected nuclei and then determining which particular assignments of peaks gave the best straight lines. The spectra show relatively sharp peaks and also indicate an effective C_2 symmetry of the complexes in solution (Table 1). The ^{1}H NMR spectra of the Tb^{III}, Dy^{III}, Ho^{III}, Tm^{III}, and Yb^{III} complexes were very complex and could not be fully assigned. However, they agree with an effective C_1 symmetry in solution. The ^{1}H NMR spectrum of the Eu^{III} complex recorded at room temperature displays very broad overlapping peaks for most protons. These results point to an increasing rigidity of the complexes in aqueous solution on decreasing the ionic radius of the Ln^{III} ion, as previously observed for other Ln^{III} complexes.[23]

The binding of a ligand to a paramagnetic Ln^{III} ion generally results in large NMR frequency shifts at the ligand nuclei, with magnitudes and signs depending critically on both the nature of the lanthanide ion and the location of the nucleus relative to the metal center.[7] Thus, the analysis of the NMR spectra of Ln^{III} paramagnetic complexes can provide useful structural information in solution. For a given nucleus i, the isotropic paramagnetic shift induced by a lanthanide ion j (δ_{ij}^{para}) is generally a combination of the Fermi contact (δ_{ij}^{con}) and dipolar (δ_{ij}^{dip}) contributions [Eq. (2)]:[7]

$$\delta_{ij}^{para} = \delta_{ij}^{exptl} - \delta_{ij}^{dia} = \delta_{ij}^{con} + \delta_{ij}^{dip} = F_i \langle S_z \rangle_j + G_i C_j \qquad (2)$$

in which the diamagnetic contribution δ_i^{dia} is obtained by measuring the chemical shifts for isostructural diamagnetic complexes (the La^{III} complex in the present case), F_i is proportional to the hyperfine coupling constant of nucleus i, G_i is the geometric factor containing the structural information, and $\langle S_z \rangle_j$ and C_j are the spin expectation value and the magnetic constant (Bleaney factor) of the paramagnetic lanthanide, respectively.[7] Dipolar shifts have been calculated with the assumption that the ligand field splitting for the lowest J state in the lanthanide complexes is small relative to kT.[24] If the principal magnetic axis is taken as the coordinate system, the dipolar contribution can be expressed as Equation (3):

$$\delta_{ij}^{dip} = D_1 \frac{3\cos^2\theta - 1}{r^3} + D_2 \frac{\sin^2\theta \cos 2\varphi}{r^3} \qquad (3)$$

in which r, θ, and φ are the spherical coordinates of the observed nucleus with respect to Ln^{III} at the origin, and D_1 and D_2 are proportional to the axial [$\chi_{zz} - {}^1/_3(\chi_{xx} + \chi_{yy} + \chi_{zz})$] and rhombic ($\chi_{xx} - \chi_{yy}$) anisotropies, respectively, of the magnetic susceptibility tensor χ.[7] In the special case of axial symmetry, the second term of Equation (3) vanishes because $D_2 = 0$. Because only the dipolar term contains geometric information about the lanthanide complex, a quantitative structural analysis requires a reliable separation of the observed paramagnetic shift into the contact and dipolar terms. The most frequently used graphical separation method is based on rearrangements of Equation (2) for each nucleus i in two linear forms [Eqs. (4) and (5)]:

$$\frac{\delta_{ij}^{para}}{\langle S_z \rangle_j} = F_i + G_i \frac{C_j}{\langle S_z \rangle_j} \qquad (4)$$

$$\frac{\delta_{ij}^{para}}{C_j} = G_i + F_i \frac{\langle S_z \rangle_j}{C_j} \qquad (5)$$

Assuming that $\langle S_z \rangle_j$ and C_j values are the same for the complexes and the free ions,[25] for which they are tabulated,[26,27], plots of $\delta_{ij}^{para}/\langle S_z \rangle_j$ against $C_j/\langle S_z \rangle_j$ and of δ_{ij}^{para}/C_j against $\langle S_z \rangle_j/C_j$ should be linear if the complexes are isostructural and possess comparable crystal field parameters. Plots of the paramagnetic shifts available for the Ln^{III} complexes of L (Ln = Ce, Pr, Nd, and Sm) follow a linear correlation according to Equations (4) and (5), indicating that the complexes are isostructural in D_2O (Figure 2). However, we notice that for Nd^{III} the experimental shifts are larger than those expected from the linear correlations obtained from Equations (4) and (5). This is probably caused by a magnification of small variations in the crystal field parameter or the geometric factors by the linearization process, because for most protons $\delta_{ij}^{para}/\langle S_z \rangle$ takes values close to zero in the Nd^{III} complex (Figure 2). Thus, we have excluded Nd^{III} from the fittings of the experimental data according to Equations (4) and (5). Samarium is not commonly used in these NMR studies, because of the small shifts induced by this ion. However, in the present case, these shifts are relatively important because the system is nonaxial (vide infra), which makes an analysis of the corresponding Sm^{III}-induced shifts possible. The agreement factors calculated according to Equation (6),[28] $0.00051 < AF_i < 0.579$, are comparable to those obtained for other Ln^{III} complexes (Table 1).[29]

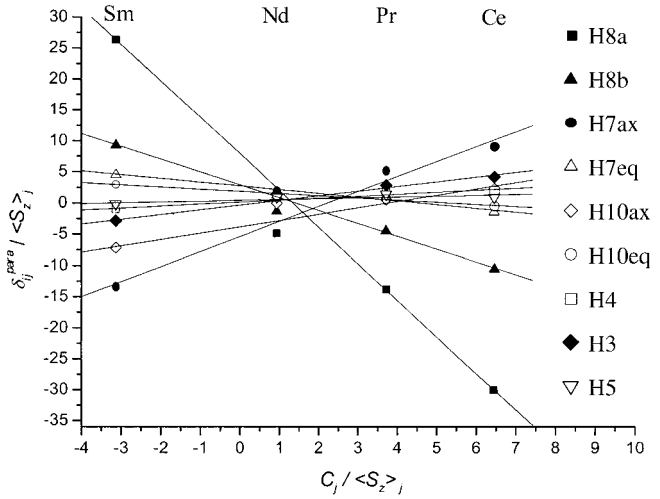

Figure 2. Plot for the separation of the contact and dipolar contributions to the observed paramagnetic shifts according to Equation (4).

$$AF_i = [\sum_j (\delta_{ij}^{exptl} - \delta_{ij}^{calcd})^2 / \sum_j (\delta_{ij}^{exptl})^2]^{1/2} \quad (6)$$

in which δ_{ij}^{calcd} are the paramagnetic shifts calculated from the G_i and F_i values listed in Table 1. Similar results are obtained when the data obtained for Nd^{III} are included in the fitting procedure. The values of the contact and dipolar contributions obtained from these plots indicate that most protons have sizable contributions from both mechanisms (Table 1), whereby the contact contribution is dominant for many proton nuclei.

Photophysical properties: In H_2O (pH 7.0), the metal complexes of L show a broad and asymmetric absorption band envelope centered around 36760 cm^{-1} (Table 2) assigned to a combination of $\pi\rightarrow\pi^*$ and $n\rightarrow\pi^*$ ligand-centered transitions.[30]

Table 2. Ligand-centered absorption and emission properties for different Ln^{III} complexes of the ligand. Energies are given in cm^{-1}.

	$\pi\rightarrow\pi^* + n\rightarrow\pi^*$[a]	$^1\pi\pi^*$[b]	$^3\pi\pi^*$[c]	$\tau(^3\pi\pi^*)$[c]
Eu	37658 (3.92)	[d]	[d]	[d]
	36807 (3.99)			
	35952 (3.84)			
Tb	37658 (3.99)	[d]	[d]	[d]
	36807 (4.05)			
	35952 (3.97)			
Gd	37658 (3.90)	24125	19474	0.92(5)
	36807 (3.99)		22988	
	35952 (3.90)		26281	

[a] Electronic spectral data in H_2O at 295 K (pH 7.0); energies are given for the maximum of the band envelope in cm^{-1}, and $\log\varepsilon$ is given within parentheses. [b] Luminescence data in H_2O at 295 K (pH 7.0). [c] Luminescence data and lifetimes [ms] in frozen H_2O solution at 77 K. [d] Luminescence quenched by transfer to the lanthanide ion.

The emission spectrum of the Gd^{III} complex recorded in H_2O (pH 7.0, 295 K) under excitation at 32258 cm^{-1} exhibits a single band (Table 2), the intensity of which quickly diminishes when a short time delay (0.05 ms) is enforced. It has thus been attributed to the $^1\pi\pi^*$ state. The absolute fluorescence quantum yield of the ligand-centered luminescence is low and amounts to $Q^L = 0.051\,\%$. The emission spectrum recorded in frozen solution (77 K) presents a second, more structured, band with a maximum at 22988 cm^{-1} and with a number of low- and high-energy shoulders (Figure 3). This band has a single exponential time decay with a lifetime of 0.92(5) ms, and is therefore assigned to the $^3\pi\pi^*$ state. The emission arising from the ligand-centered $^3\pi\pi^*$ state completely disappears for the Eu^{III} and Tb^{III} complexes (Figure 3), indicating sensitization of the metal ions as a result of a $^3\pi\pi^*$-to-metal energy transfer. The emission spectrum of a 10^{-3} M solution of the Eu^{III} complex in H_2O at pH 7 and 295 K, obtained under excitation at 22988 cm^{-1}, displays the typical $^5D_0\rightarrow{}^7F_J$ transitions at 17200, 16855, 16227, 15361, and 14571 cm^{-1} for $J = 0$, 1, 2, 3, and 4, respectively. The absolute quantum yield of the metal-centered luminescence in H_2O at pH 7 amounts to 0.3 %.

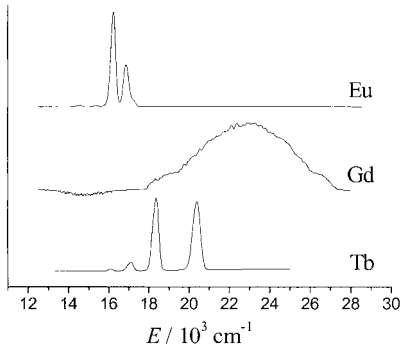

Figure 3. Phosphorescence spectra of ligand complexes (ν_{exc} = 22988 cm^{-1}). The spectra of the Eu^{III} and Tb^{III} complexes were recorded from 10^{-3} M solutions in water at 295 K, while the spectrum of the Gd^{III} complex was recorded from a 10^{-6} M solution in water frozen at 77 K. Vertical scale: arbitrary units.

Reinhoudt and co-workers[31] have concluded from their work on modified Eu^{III}-containing calix[4]arenes that the antenna effect is improved when the $^3\pi\pi^*$ 0-phonon transition lies 3500 cm^{-1} above the Ln^{III} excited state. They also observed that the $^1\pi\pi^*\rightarrow{}^3\pi\pi^*$ intersystem crossing is maximized when the energy difference between these states amounts to $\approx$5000 cm^{-1}. A similar conclusion was reached by Latva et al.,[32] who found that the best energy-transfer efficiency is obtained when the 0-phonon band of $^3\pi\pi^*$ lies at 21000–22000 cm^{-1}. In the case of our Eu^{III} complex of L, we note the following facts: 1) the $^1\pi\pi^*-{}^3\pi\pi^*$ energy difference amounts to only 1137 cm^{-1} and 2) the 0-phonon transition of the ligand $^3\pi\pi^*$ state (as measured for the Gd complex at 77 K) lies at 26281 cm^{-1}, leading to a $\Delta E(^3\pi\pi^*-{}^5D_0)$ difference equal to 9081 cm^{-1}. This data clearly explains the poor sensitization of Eu^{III} by L, since the 0-phonon transition of the ligand $^3\pi\pi^*$ state lies at very high energy, while the energy difference between the ligand $^1\pi\pi^*$ and $^3\pi\pi^*$ states is too small to favor $^1\pi\pi^*\rightarrow{}^3\pi\pi^*$ intersystem crossing.

The spectrum of a solution of the Tb^{III} complex in water, recorded under analogous conditions, shows the typical $^5D_4\rightarrow{}^7F_J$ transitions at 20386, 18360, 17076, and 16089 cm^{-1} for $J = 6$, 5, 4, and 3, respectively. For the Tb^{III} complex, the

$\Delta E(^3\pi\pi^* - ^5D_4)$ difference amounts to 5743 cm^{-1}. Taking the latter value into account, one expects a better antenna effect for the Tb^{III} complex than for the Eu^{III} one, and this is indeed observed: the absolute quantum yield of the metal-centered luminescence in H_2O at pH 7 amounts to 1.9%, $\approx$6 times larger than for Eu^{III}.

The emission lifetimes of the Eu($^5D_0$) and Tb($^5D_4$) excited levels have been measured in D_2O and H_2O (10^{-3} M solutions). They were used to calculate the number of coordinated water molecules q by means of Equations (7) and (8) for Eu and Tb, respectively.[33]

$$q = 1.05\,\Delta k_{obs} \quad (7)$$

$$q = 4.2\,\Delta k_{obs} \quad (8)$$

In these equations $\Delta k_{obs} = k_{obs}(H_2O) - k_{obs}(D_2O)$ (k_{obs} is given in ms^{-1}) and $k_{obs} = 1/\tau_{obs}$. The measured emission lifetimes in H_2O solutions ($\tau_{obs}(H_2O)$) were 0.56 ± 0.01 (Eu) and 1.59 ± 0.01 ms (Tb), while the $\tau_{obs}(D_2O)$ values amount to 2.04 ± 0.01 (Eu) and 2.27 ± 0.01 ms (Tb). With Equations (7) and (8), we obtain $q = 1.3$ (Eu) and 0.8 (Tb), with an estimated uncertainty of ± 0.5 for q. These equations were established from crystalline complexes in which interactions generated by molecules of water in the second coordination sphere are absent. Consequently, we have also made use of Equations (9) and (10), proposed by Beeby et al.[34] for solutions of poly(aminocarboxylate) complexes with $q \leq 1$, whereby q^N is the number of NH oscillators when amide groups are coordinated to the metal ion.

$$q = 1.2\,(\Delta k_{obs} - 0.25 - 0.075\,q^N) \quad (9)$$

$$q = 5.0\,(\Delta k_{obs} - 0.06) \quad (10)$$

When $q^N = 0$, we obtained $q = 1.2$ and 0.7 for Eu and Tb, respectively. Quite recently, a refined Equation (11)[35] has been proposed for Eu complexes in solution, with an estimated uncertainty of ± 0.1 for q.

$$q = 1.11\,(\Delta k_{obs} - 0.31 - 0.075\,q^N) \quad (11)$$

In our case, this equation yields $q = 1.1$. All these results point to the complexes having one coordinated water molecule in aqueous solution.

Ab initio calculations: The $[Ln(L)(H_2O)]^-$ systems (Ln = La, Pr, or Gd) were investigated both in vacuo and in aqueous solution by means of ab initio calculations at the HF level. In the case of Gd^{III} complexes, the long electronic relaxation time of the metal ion prevents any observation of NMR spectra, and, for this reason, their solution structures and properties have to be deduced from the NMR spectra of complexes with other lanthanides. Theoretical calculations provide direct information on gadolinium systems as well as on those dynamic processes that are usually too fast to be observed on the NMR timescale, such as the water exchange process. As there is not a good all-electron basis set for lanthanides, the effective core potential (ECP) of Dolg et al. and the related [5s4p3d]-GTO valence basis set was applied in these calculations.[36] This ECP includes $46 + 4f^n$ electrons in the core, leaving the outermost 11 electrons to be treated explicitly; it has been demonstrated that this method provides reliable results for the lanthanide–aqua ions,[37] several lanthanide complexes with polyamino carboxylate ligands,[38,39] and lanthanide dipicolinates.[40] In contrast to all-electron basis sets, ECPs account to some extent for relativistic effects, which are believed to become important for the elements from the fourth row of the periodic table.

Our ab initio calculations provide a minimum energy conformation in which the ligand wraps itself around the metal ion by twisting the pyridyl units relative to each other, so that the pyridine nitrogen atoms and the metal are not linear (Figure 4), with an N_{PY}-Ln-N_{PY} angle of 162–165°. In these structures, the carboxylate pendant arms are situated alternately above and below the planes of the pyridyl units. The complexes present two different sources of chirality: one arising from the two five-membered rings formed by the binding of the acetate arms to the ion (absolute configuration Δ or Λ) and the other to the five-membered ring formed by the binding of the ethylene diamino moiety (absolute configuration δ or λ). The minimum energy conformations obtained for $[Ln(L)(H_2O)]^-$ both in vacuo and in solution correspond to $\Delta(\lambda)$ (or $\Lambda(\delta)$) conformations.

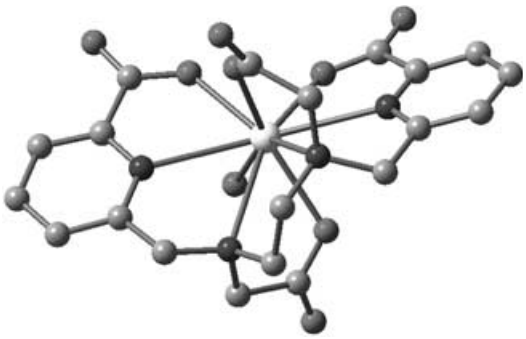

Figure 4. The structure of the $[Pr(L)(H_2O)]^-$ complex optimized in aqueous solution (CPCM model) at the HF/3-21G* level. Hydrogen atoms are omitted for simplicity.

The calculated bond lengths between the ion and the coordinated ligand atoms (Table 3) decrease along the lanthanide series, as is usually observed for Ln^{III} complexes.[23] The in vacuo-optimized structures exhibit bond lengths Ln–N_{AM} and Ln–N_{PY} (N_{AM} = amine nitrogen atom, N_{PY} = pyridyl nitrogen atom) that are longer than those usually observed for Ln^{III} complexes with polyamino carboxylate ligands, while the Ln–O bonds are close to the experimental ones. In solution, Ln–N bond lengths are shorter whereas Ln–O bond lengths are slightly increased, providing a general better agreement with typical experimental bond lengths obtained for polyamino carboxylate chelates.[41,42] The Gd–O_W bond length obtained for the optimized structure in solution (2.492 Å) is in excellent agreement with that normally assumed in the analysis of the ^{17}O NMR longitudinal relaxation data (2.5 Å). The coordinated water molecule is bent, which results in an averaged Gd···H_W distance of 2.969 Å. This distance is close to the range recently reported by Car-

Table 3. Values of the main geometrical parameters (bond lengths [Å], angles [°]) of calculated (in vacuo and in aqueous solution) structures for $[Ln(L)(H_2O)]^-$ complexes at the HF/3-21G* level.[a]

		In vacuo	In solution
La	La–N_{AM}	2.96(8)	2.84(2)
	La–N_{PY}	2.812(2)	2.784(6)
	La–O_{COO}	2.43 (1)	2.45(3)
	La–O_{PYCOO}	2.45(4)	2.49(2)
	La–O_W	2.652	2.600
	N_{PY}-La-N_{PY}	162.07	165.51
	O_{COO}-La-O_{COO}	136.70	142.27
Pr			
	Pr–N_{AM}	2.94(9)	2.80(2)
	Pr–N_{PY}	2.781(5)	2.746(6)
	Pr–O_{COO}	2.40(2)	2.40(2)
	Pr–O_{PYCOO}	2.43(4)	2.46(2)
	Pr–O_W	2.616	2.569
	N_{PY}-Pr-N_{PY}	162.10	166.53
	O_{COO}-Pr-O_{COO}	137.55	143.75
Gd			
	Gd–N_{AM}	2.9(1)	2.77(3)
	Gd–N_{PY}	2.73(2)	2.688(7)
	Gd–O_{COO}	2.32(2)	2.32(2)
	Gd–O_{PYCOO}	2.35(4)	2.39(3)
	Gd–O_W	2.538	2.492
	N_{PY}-Gd-N_{PY}	160.68	164.99
	O_{COO}-Gd-O_{COO}	138.24	145.61

[a] The average values are reported with standard deviations in parentheses. N_{AM} = amine nitrogen atoms, N_{PY} = pyridyl nitrogen atoms, O_{COO} = aliphatic carboxylate oxygen atoms, O_{PYCOO} = aromatic carboxylate oxygen atoms, O_W = water oxygen atoms.

avan et al.[43] for different MRI contrast agents (3.1 ± 0.1 Å). Optimized Cartesian coordinates obtained for the different $[Ln(L)(H_2O)]^-$ systems both in vacuo and in solution are given in the Supporting Information.

The ^{13}C NMR shielding constants of the $[La(L)(H_2O)]^-$ complex were calculated for the structures optimized both in vacuo and in solution by means of the GIAO method. The main results of these calculations together with the experimental values are given in Table 4.

The calculations of the NMR shielding constants were performed at the B3LYP/6-311G** level with the 46 core electron ECP by Stevens et al.[44] In general, there is an excellent agreement between the experimental and calculated chemical shifts, as indicated by the agreement factors obtained [Eq. (12)]:

$$AF_j = [\sum_i (\delta_{ij}^{exptl} - \delta_{ij}^{calcd})^2 / \sum_i (\delta_{ij}^{exptl})^2]^{1/2} \quad (12)$$

in which δ_{ij}^{exp} and δ_{ij}^{calcd} are the experimental and calculated chemical shift values for a nucleus i of a given lanthanide complex j. The agreement between experimental and calculated shifts is slightly better when calculations are performed on the structure optimized in aqueous solution ($AF_j = 0.0295$) than when they are carried out on the structure optimized in vacuo ($AF_j = 0.0323$). These results indicate that our ab initio calculations provide reasonably good models for the structure of these complexes in solution, especially when solvent effects are included. Calculations of the ^{13}C NMR shielding constants on the structure optimized in solution at the HF/6-311G** level result in a poor agreement between the experimental and calculated shifts (Table 4). These results highlight the importance that inclusion of electronic correlation effects has on these calculations.

Table 4. Experimental and calculated (GIAO method) ^{13}C NMR chemical shifts for the $[La(L)(H_2O)]^-$ complex (see Scheme 1 for labeling).

	$\delta_{i,exptl}$[a]	$\delta_{i,calcd}$[b]	$\delta_{i,calcd}$[c]	$\delta_{i,calcd}$[d]
C1	174.8	170.7	172.2	168.7
C2	153.1	162.5	160.7	189.5
C3	125.6	127.0	126.9	149.1
C4	141.9	140.2	140.7	162.2
C5	127.6	124.6	124.2	136.0
C6	158.7	163.1	162.1	183.5
C7	59.8	63.6	64.9	54.7
C8	62.7	65.9	66.2	76.8
C9	181.1	176.9	177.1	179.3
C10	55.1	56.5	57.8	49.5
AF_j[e]		0.0323	0.0295	0.137

[a] Assignment supported by 2D HMQC and HMBC experiments at 298 K in D_2O (pH 7.0). [b] Values calculated on the structure optimized in vacuo at the B3LYP/6-311G** level. [c] Values calculated on the structure optimized in solution at the B3LYP/6-311G** level. [d] Values calculated on the structure optimized in solution at the HF/6-311G** level. [e] Agreement factors calculated according to Equation (12).

Pr^{III}-induced shifts and relaxation-rate enhancement effects: The atomic coordinates obtained from our ab initio calculations for the $[Pr(L)(H_2O)]^-$ system (both in vacuo and in solution) were used to assess the agreement between the experimental and predicted Pr^{III}-induced dipolar shifts by means of the shift analysis method.[45] The experimental Pr^{III}-induced dipolar shifts were taken as $\delta_{ij}^{dip} = G_i C_j$ [(Eq. (2)] for each proton, whereby the experimental values of G_i were obtained from the corresponding Reilley plots [Eqs. (4) and (5)]. The shift analysis program calculates the dipolar shifts defined by Equation (3) in the molecular coordinate system by means of a linear least-squares search that minimizes the difference between the experimental and calculated data. Table 5 shows a comparison between the experimental and calculated dipolar shifts values for the Pr^{III} complex.

The agreement between the experimental and calculated isotropic shifts obtained from the structure optimized in vacuo of $[Pr(L)(H_2O)]^-$ is reasonably good, as indicated by the agreement factor obtained [$AF_j = 0.149$, Eq. (12)]. However, a much better agreement between the experimental and calculated dipolar shifts was obtained when the atomic coordinates of the structure optimized in solution were used. An excellent agreement factor AF_j of 0.083 was obtained, with D_1 and D_2 values amounting to 2184 ± 89 and -1917 ± 169 ppm Å^3, respectively. Similar agreement factors were previously obtained for Ln^{III} texaphyrins ($0.066 < AF_j < 0.259$).[46] As expected for a nonaxial system, the D_1 and D_2 values obtained define very large χ tensor anisotropies.[19] These results indicate that our ab initio calculations provide good models for the structure of these complexes in solution, particularly when solvent effects are taken into account. These D_1 and D_2 values calculated from the paramagnetic shifts of proton nuclei were used to determine the dipolar shifts for carbon atoms with Equation (3) (Table 5). Subsequently, the contact shifts were obtained by subtract-

Table 5. Comparison of experimental and calculated dipolar ^{1}H shifts and calculated dipolar and contact ^{13}C NMR shifts in $[Pr(L)(H_2O)]^-$.[a]

	$\delta^{con}_{i,exp}$(Pr)	$\delta^{dip}_{i,exp}$(Pr)	$\delta^{dip}_{i,calcd}$(Pr)[b]	$\delta^{dip}_{i,calcd}$[c]		$\delta^{dip}_{i,calcd}$	$\delta^{con}_{i,calcd}$
H3	0.89	−8.36	−8.41	−9.16	C_1	−42.1	16.1
H4	−0.59	−3.52	−3.89	−3.98	C_2	−36.5	4.1
H5	−1.48	−1.54	−3.03	−2.40	C_3	−13.0	−10.1
H7ax	15.67	−26.40	−23.28	−23.15	C_4	−7.0	2.0
H7eq	−8.28	6.60	0.63	4.20	C_5	−5.9	−11.3
H8a	−23.94	64.76	66.57	66.37	C_6	−9.3	−9.1
H8b	−12.09	25.19	19.44	22.72	C_7	−3.4	−1.0
H10ax	11.23	−11.00	−6.16	−9.13	C_8	59.4	−12.5
H10eq	−5.56	3.74	−0.76	0.621	C_9	42.7	−3.7
D_1[ppm Å^3]			1998 ± 140	2184 ± 90	C_{10}	−2.8	16.9
D_2[ppm Å^3]			−1715 ± 270	−1917 ± 169			
AF_j			0.149	0.083			

[a] Positive values correspond to shifts to higher fields. [b] Values calculated with the structure of the $[Pr(L)(H_2O)]^-$ complex optimized in vacuo at the HF/3-21G* level. [c] Values calculated with the structure of the $[Ln(L)(H_2O)]^-$ complex optimized in aqueous solution at the HF/3-21G* level.

ing the calculated dipolar contributions from the measured isotropic shifts. Table 5 also gives the contact contributions for proton nuclei in $[Pr(L)(H_2O)]^-$ calculated as $\delta^{con}_{ij} = F_i\langle S_z\rangle_j$. The theoretical value for the ratio of the contact to pseudocontact contributions in Pr^{III} compounds is 0.269,[7] and, therefore, the hyperfine ^{1}H and ^{13}C NMR shifts in Pr^{III} complexes are expected to be largely pseudocontact in origin. However, the data reported in Table 5 show that both proton and carbon nuclei have important contact contributions for the Pr^{III} complex; this suggests an important spin density delocalization onto the ligand backbone.

Further information on the structure of the complexes in solution was obtained from Pr^{III}-induced relaxation-rate enhancements in the ^{1}H nuclei of the ligand. The Pr^{III}-induced ^{1}H NMR relaxation enhancements for L were measured at 7.05 T and 298 K (Table 6). In order to correct for diamagnetic contributions, the relaxation rates for the corresponding La^{III} complex were subtracted from the measured values of the Pr^{III} complex (Table 6). The electron relaxation for Pr^{III} is very fast ($T_{1e} \approx 10^{-13}$ s) and, consequently, the contact contribution to the paramagnetic relaxation is negligible. Two contributions are of importance: the "classical" dipolar relaxation and the Curie relaxation. Equation (13) can be derived from a simplified Solomon–Bloembergen equation[47] and the equation for the Curie relaxation (assuming extreme narrowing):[48,49]

$$\frac{1}{T_1} = \left[\frac{4}{3}\left(\frac{\mu_0}{4\pi}\right)^2 \mu^2\gamma_I^2\beta^2 T_{1e} + \frac{6}{5}\left(\frac{\mu_0}{4\pi}\right)^2 \frac{\gamma_I^2 H_0^2 \mu^4 \beta^4}{(3kT)^2}\tau_R\right]\frac{1}{r^6} + \frac{1}{T_{1OS}} \quad (13)$$

in which the first term between the brackets represents the "classical" dipolar contribution, and the second term describes the Curie relaxation. Here, $\mu_0/4\pi$ is the magnetic permeability in a vacuum, μ is the effective magnetic moment of the lanthanide ion, γ_I is the gyromagnetic ratio of the nucleus under study, β is the Bohr magneton, T_{1e} is the electron spin relaxation time, r is the distance between the ^{1}H nucleus in question and the lanthanide ion, H_0 is the magnetic field strength, k is the Boltzmann constant, T is the temperature, τ_R is the rotational tumbling time of the complex, and $1/T_{1OS}$ represents the outer-sphere contribution. The contribution of the Curie spin mechanism to the total relaxation becomes significant for larger molecules (τ_R increases), particularly at higher fields. At constant temperature and B_0, application of Equation (13) allows the determination of relative r values in the complexes without the need to estimate T_{1e} and τ_R, which would be needed to calculate absolute distances. A plot of $1/T_1$ versus $1/r^6$, whereby r are the Pr···H distances obtained from the ab initio-optimized structure in an aqueous solution, gives a straight line with a gradient $k = 1.25 \pm 0.07 \times 10^{-55}$ m^{6}s^{-1} and an intercept of 1.3 ± 0.9 s^{-1} ($R^2 = 0.991$). The gradient obtained from this plot represents the term between the brackets in Equation (13), while the intercept represents the outer-sphere contribution ($1/T_{1OS}$), which becomes significant only for remote nuclei. Inserting $T_{1e} = 0.57 \times 10^{-13}$ s[7] and the τ_R value obtained from the analysis of the NMRD and ^{17}O NMR data ($\tau_R = 55$ ps, see later) we obtain $k = 8.09 \times 10^{-56}$ m^{6}s^{-1}, which is in reasonable agreement with the experimental value considering the uncertainties in these values. The experimental values of k and $1/T_{1OS}$ were used to obtain experimental Pr···H distances in solution from relaxation data by means of Equation (13). In general, the experimental Pr···H distances are in satisfactory agreement with those obtained from the theoretical calculations (Table 6), thereby confirming that the computational approach provides a reliable description of the solution structure.

Table 6. Pr···H distances calculated from ^{1}H NMR relaxation data for 40 mM solutions of Ln^{III} complexes in D_2O (300 MHz, 25 °C, pD = 7).

	$1/T_{1(Pr)}$[s^{-1}]	$1/T_{1(La)}$[s^{-1}]	r[Å][a]	r[Å][b]
H3	8.696	0.911	5.633	5.19
H4	4.000	0.989	6.660	6.50
H5	6.024	1.224	5.773	5.75
H7ax	43.478	5.128	3.895	3.87
H7eq	16.667	5.435	4.663	4.83
H8a	41.667	4.219	3.761	3.89
H8b	16.129	3.559	4.518	4.73
H10ax	[c]	5.319	3.714	[c]
H10eq	17.615	5.618	4.586	4.77

[a] Pr^{III}···H distances obtained from ab initio calculations in aqueous solutions. [b] Pr^{III}···H distances obtained from experimental ^{1}H NMR relaxation data. [c] Not obtained.

Variable-temperature ^{17}O NMR and NMRD measurements: The relaxivity describes the efficiency of magnetic dipolar coupling occurring between the solvent nuclei and the paramagnetic metal ion, and represents a measure of the efficacy of the complex as a contrast agent. The relaxation rates of

the bulk water protons in the vicinity of a paramagnetic ion are enhanced as a result of long- (outer-sphere relaxation) and short-range interactions (inner-sphere relaxation). The latter is governed by the rotational correlation time of the complex (τ_R), the residence time of a water proton in the inner coordination sphere (τ_m), and the electronic longitudinal and transverse relaxation rates ($1/T_{1e}$ and $1/T_{2e}$) at the metal center. As pointed out previously,[50] it is difficult to calculate the parameters that determine the relaxivity of a given compound from nuclear magnetic resonance dispersion (NMRD) profiles without obtaining independent information of at least some of the most important parameters. Therefore, we measured variable-temperature ^{17}O NMR shifts and relaxations in a 0.153 M solution of the $[Gd(L)(H_2O)]^-$ chelate in H_2O (pH 6.38). The temperature dependence of the reduced longitudinal relaxation rates ($1/T_{1r}$), transversal relaxation rates ($1/T_{2r}$), and reduced chemical shifts ($\Delta\omega_r$) for $[Gd(L)(H_2O)]^-$ is shown in Figure 5. Although the full equations given in the Supporting Information were used to fit the experimental ^{17}O NMR data, it is useful to consider the simplified Equations (14) and (15) for the reduced relaxation rates, whereby the contribution to $1/T_{2r}$ of the chemical shift difference between the bound and bulk water, $\Delta\omega_m$, has been neglected.

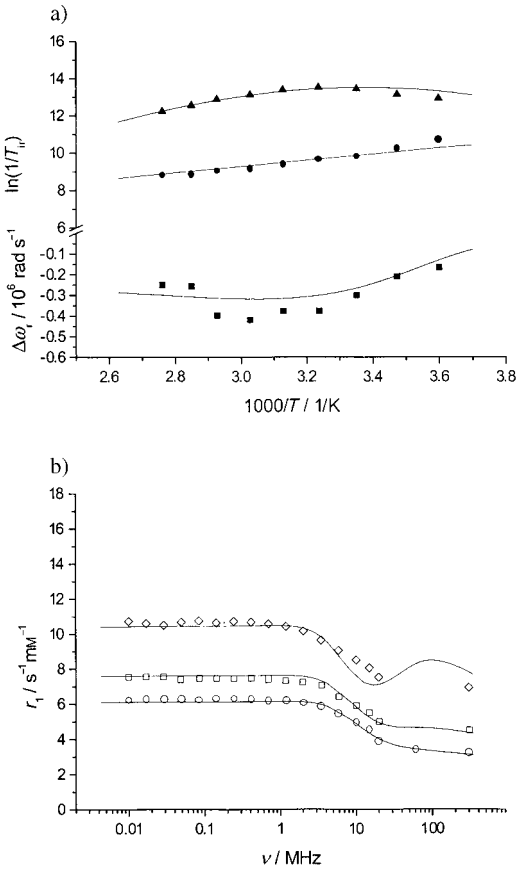

Figure 5. a) Longitudinal (●) and transverse (▲) ^{17}O relaxation rates and ^{17}O chemical shifts (■) of $[Gd(L)(H_2O)]^-$ at 7.05 T and pH 6.38; b) ^1H NMRD profiles of $[Gd(L)(H_2O)]^-$ at 5, 25 and 37 °C (from top to bottom) and pH 6.6.

$$\frac{1}{T_{1r}} = \frac{1}{T_{1m} + \tau_m} \quad (14)$$

$$\frac{1}{T_{2r}} = \frac{1}{T_{2m} + \tau_m} \quad (15)$$

In these equations $1/T_{1m}$, $1/T_{2m}$ are the relaxation rates in the bound water. Since τ_m decreases, while T_{1m} and T_{2m} generally increase with increasing temperature, the sign of the temperature dependence of $1/T_{1r}$ and $1/T_{2r}$ will depend on which term dominates in the denominator of Equations (14) and (15). The maximum observed in the temperature dependence of $1/T_{2r}$ (Figure 5a) is characteristic of a changeover from the "fast exchange" limit at high temperature, whereby T_{2m} is the principal term in the denominator of Equation (15), to the slow exchange limit at low temperatures. Because $T_{1m} > T_{2m}$, the maximum observed in $1/T_{2r}$ is not observed for $1/T_{1r}$, which is within the fast exchange region for the whole range of experimentally available data from different temperatures.

The $[Gd(L)(H_2O)]^-$ chelate was investigated by water ^1H longitudinal relaxation-time measurements at 5, 25, and 37 °C and magnetic field strengths varying between 2.3474×10^{-4} and 7.05 T (NMRD). Longitudinal proton relaxation enhancements in NMRD studies are commonly expressed in relaxivities (r_1, in $s^{-1}mM^{-1}$). The curves obtained for $[Gd(L)(H_2O)]^-$ are included in Figure 5b. The temperature dependence of the NMRD profile usually gives a good indication of which parameters limit the proton relaxivity. If the high field value (>10 MHz) does not decrease with increasing temperature, relaxivity is limited by slow water exchange, whereas in the opposite case, fast rotation is the limiting factor. For $[Gd(L)(H_2O)]^-$, the relaxivity increases with decreasing temperature; this shows that the relaxivity is dominated by fast rotation, as is usually observed for small Gd^{III} chelates.[50]

A simultaneous fitting of the NMRD and ^{17}O NMR data of $[Gd(L)(H_2O)]^-$ was performed with sets of equations usually used to predict variable-temperature ^{17}O NMR data, with the Solomon—Bloembergen–Morgan equations (which describe the field dependency of the inner-sphere relaxivity, r_1) and with the Freed equation for the outer-sphere contribution of the relaxivity.[2] The set of equations used is given in the Supporting Information. Following previous studies, the distance of closest approach for the outer-sphere contribution a_{GdH} was set to 3.5 Å. The distance between the protons of the coordinated water molecules and the Gd^{III} ion (r_{GdH}) was fixed at 2.969 Å, which corresponds to the averaged r_{GdH} distance obtained from our ab initio calculation in aqueous solution (vide supra). On the basis of our ab initio calculations, the r_{GdO} distance was fixed at 2.492 Å. The number of water molecules in the first coordination sphere of Gd^{III} (q) was taken as 1.0. Finally, the value of E_v, the activation energy of the correlation time τ_v, was fixed at 1 kJ mol^{-1}.[50] Attempts to unfix this parameter led to negative values of the activation energy. The parameters obtained from the fittings are listed in Table 7 with the curve fits shown in Figure 5. For comparison, previously reported data for $[Gd(dota)(H_2O)]^-$ and $[Gd(dtpa)(H_2O)]^{2-}$ have been included in Table 7.[50]

Table 7. Parameters obtained from the simultaneous analysis of ^{17}O NMR and NMRD for the $[Gd(L)(H_2O)]^-$ complex.[a]

Parameter	$[Gd(L)(H_2O)]^-$	$[Gd(dota)(H_2O)]^-$	$[Gd(dtpa)(H_2O)]^{2-}$
k_{ex}^{298} [10^6 s^{-1}]	5.0 ± 0.6	4.1 ± 0.2	3.3 ± 0.2
$\Delta H^{\neq}$ [kJ mol^{-1}]	40.1 ± 2.4	49.8 ± 1.5	51.6 ± 1.4
$A/\hbar$ [10^6 rad s^{-1}]	-2.31 ± 0.08	-3.7 ± 0.2	-3.8 ± 0.2
τ_R^{298} [ps]	55 ± 10	77 ± 4	58 ± 11
E_R [kJ mol^{-1}]	17.9 ± 1.6	16.1 ± 7.4	17.3 ± 0.8
τ_v^{298} [ps]	12.6 ± 0.8	11 ± 1	25 ± 1
E_V [kJ mol^{-1}]	1.0[b]	1.0[b]	1.6 ± 1.8
Δ^2 [10^{20} s^{-2}]	1.2 ± 0.1	0.16 ± 0.01	0.46 ± 0.02
D_{GdH}^{298} [10^{-10} $m^2 s^{-1}$]	19 ± 3	22 ± 1	20 ± 3
E_{DGdH} [kJ mol^{-1}]	30.1 ± 2.1	20.2 ± 1.1	19.4 ± 1.8
$\chi(1+\eta^2/3)^{1/2}$ [MHz]	17 ± 2	10 ± 1	14 ± 2

[a] The data listed for $[Gd(dtpa)(H_2O)]^{2-}$ and $[Gd(dota)(H_2O)]^-$ have been reported previously in Ref. [50] and are provided here for comparison. [b] Parameters fixed during the fitting procedure.

Inspection of the data listed in Table 7 reveals some similarities in the parameters that determine the relaxivity in the three complexes. Indeed, the values obtained for the rotational correlation time (τ_R^{298}) are in reasonable agreement, and they are typical of small Gd^{III} chelates. Moreover, values of the relative diffusion coefficient D_{GdH}^{298} are also very similar, as expected for systems of similar bulk. The parameters describing the electronic relaxation of the Gd^{III} ion are expressed in terms of the zero-field splitting interaction (τ_v^{298}, E_v and Δ^2). The value determined from the fittings for τ_v^{298} is close to that reported for $[Gd(dota)(H_2O)]^-$, while that of Δ^2 is larger; however, it is still within the range normally observed for Gd^{III} chelates.[3]

The value obtained for the scalar coupling constant ($A/\hbar$), is smaller than those reported for other Gd^{III} polyaminocarboxylate complexes that have one inner-sphere water molecule (typically -3.8×10^6 rad s^{-1}).[50] The shift induced by a Gd^{III} complex to the water ^{17}O resonance is proportional to q, if the exchange between Gd^{III}-bound water and the bulk is rapid on the NMR timescale.[7] Therefore, the small value obtained for $A/\hbar$ could reflect a q value lower than one, caused by the presence of a hydration equilibrium. However, we do not exclude the possibility that an efficient spin delocalization on the ligand backbone, caused by the presence of aromatic units, could have an effect on $A/\hbar$ for the coordinated water molecule.

Whereas an ideal value of k_{ex}^{298} can be calculated to be $\approx 3 \times 10^7$ s^{-1} at 25 °C, both $[Gd(dota)(H_2O)]^-$ and $[Gd(DTPA)(H_2O)]^{2-}$ have a water exchange rate that is ≈ 10 times slower. The water exchange rate (k_{ex}^{298}) determined for $[Gd(L)(H_2O)]^-$ is slightly more favorable than that reported for chelates, such as $[Gd(dota)(H_2O)]^-$ and $[Gd(dtpa)(H_2O)]^{2-}$, and one order of magnitude faster than for DTPA–bis(amide) chelates.

Conclusion

In this work, we present a new polyaminocarboxylate ligand that contains pyridine units and which shows promise as a Ln^{III} chelating agent. This ligand can sensitize both the Eu^{III} and Tb^{III} luminescence; however, the quantum yields of the Eu^{III}- and Tb^{III}-centered luminescence remain modest on account of a relatively inefficient energy transfer from the pyridine moieties to the Ln^{III} ion. The corresponding Gd^{III} complex is nine-coordinate, whereby a water molecule completes the metal-ion coordination sphere. This induces a relaxivity in solutions of the complex at the imaging fields (5.0 s^{-1} mM^{-1} at 20 MHz and 25 °C) that is somewhat larger than those reported for the standard contrast agents (4.74 and 4.69 s^{-1} mM^{-1} at 20 MHz and 25 °C for $[Gd(dota)(H_2O)]^-$ and $[Gd(dtpa)(H_2O)]^{2-}$, respectively). These favorable relaxation properties open interesting perspectives for the design of new and more efficient contrast agents for MRI by, for instance, introducing appropriate functions in the pyridine rings.

Experimental Section

Solvents and starting materials: Dimethyl pyridine-2,6-dicarboxylate was prepared according to the literature method.[51] The chloride and nitrate salts, $LnCl_3 \cdot n H_2O$ and $Ln(NO_3)_3 \cdot n H_2O$, were purchased from Aldrich and Alfa Laboratories, and were used without further purification. Solvents and starting materials were purchased from Aldrich and used without further purification, unless otherwise stated. Silica gel (Fluka 60, 0.063–0.2 mm) was used for preparative column chromatography. D_2O for NMR studies was obtained from Merck (99.9 %D). Samples of the Ln^{III} complexes for the NMR measurements were prepared by dissolving equimolar amounts of ligand and hydrated $Ln(NO_3)_3$ in D_2O followed by adjustment of the pD with ND_4OD and DCl (Aldrich) solutions in D_2O. Samples for NMRD and ^{17}O NMR measurements were prepared by dissolving the appropriate amounts of ligand and hydrated $LnCl_3$ in H_2O. pH values were adjusted with the aid of dilute solutions of NaOH and HCl. The pH of the solutions was measured at room temperature with a calibrated microcombination probe purchased from Aldrich Chemical Co. The pH values given are direct meter readings without correction for D-isotope effects.

Physical methods: Elemental analyses were carried out on a Carlo Erba 1108 elemental analyzer. FAB mass spectra were recorded on a FISONS QUATRO mass spectrometer with a Cs ion gun and 3-nitrobenzyl alcohol as the matrix. IR spectra were recorded, as KBr discs or Nujol mulls, on a Bruker Vector 22 spectrophotometer. Electronic spectra in the UV/Vis range were recorded at 20 °C on a Perkin–Elmer Lambda 900 UV/Vis spectrophotometer in 1.0 cm quartz cells. Excitation and emission spectra were recorded on a Perkin–Elmer LS-50B spectrometer equipped for low-temperature (77 K) measurements. Lifetimes are averages of at least 3–5 independent determinations. Absolute quantum yields were calculated relative to quinine sulfate in dilute sulfuric acid (absolute quantum yield: 0.546).[52]

^1H and ^{13}C NMR spectra were recorded at 25 °C on Bruker AC200F and Bruker WM-500 spectrometers. For measurements in D_2O, *tert*-butyl alcohol was used as an internal standard with the methyl signal calibrated at $\delta = 1.2$ (^1H) and 31.2 ppm (^{13}C). Spectral assignments were based in part on two-dimensional COSY, HMQC, and HMBC experiments. ^{17}O NMR spectra and ^1H NMR T_1 values were obtained on a Varian INOVA-300 spectrometer. D_2O (100 %) was used as an external chemical shift reference for ^{17}O resonances. Longitudinal ^1H and ^{17}O relaxation times T_1 were measured by the inversion–recovery pulse sequence,[53] and

the transverse relaxation times (T_2) were obtained by the Carr–Purcell–Meiboom–Gill spin-echo technique.[54] The $1/T_1$ nuclear magnetic resonance dispersion (NMRD) profiles were recorded at 5, 25, and 37 °C with a Stelar field cycling system covering a range of magnetic fields from 2.3474×10^{-4} to 0.35 T (corresponding to a proton Larmor frequency range of 0.01–15 MHz). Additional points at 20, 60, and 300 MHz were obtained on Minispec PC-20, Minispec mq-60 and Bruker AMX-300 spectrometers, respectively.

Methyl 6-formylpyridine-2-carboxylate (1): $NaBH_4$ (7.3 g, 0.193 mol) was added to a stirred solution of dimethyl pyridine-2,6-dicarboxylate (10.0 g, 0.051 mol) in MeOH (400 mL) at 0 °C. The solution was stirred for 3 h at 0 °C and then poured into a saturated $NaHCO_3$ aqueous solution (200 mL). The bulk of the methanol was evaporated, and the resulting aqueous solution was extracted with $CHCl_3$ (5×100 mL). The combined organic phases were dried over $MgSO_4$ and evaporated to dryness. The residue was dissolved in dioxane (200 mL), and SeO_2 (2.8 g, 0.025 mol) was added. The solution was heated at reflux for 2.5 h, filtered while hot, and evaporated to dryness. The crude residue was purified by column chromatography (SiO_2, $CHCl_3$) to give 5.7 g (70 %) of **1** as a pale yellow solid. ^{1}H NMR (200 MHz, $CDCl_3$, 25 °C, TMS): $\delta=10.19$ (s, 1H; -CHO,), 8.35 (dd, $^3J(H,H)=7.3$ Hz, $^4J(H,H)=1.5$ Hz, 1H; py), 8.14 (m, 2H; Py), 4.06 ppm (s, 3H; -OCH_3); ^{13}C NMR (50.4 MHz, $CDCl_3$, 25 °C, TMS): $\delta=$ 53.2 (primary C), 192.6, 129.0, 128.0, 124.3 (tertiary C), 164.0, 152.7, 148.6 ppm (quaternary C); elemental analysis calcd (%) for $C_8H_7NO_3$ (165.2): C 58.2, H 4.3, N 8.5; found: C 57.7, H 4.4, N 8.2; IR (KBr): $\tilde{\nu}=$ 1719 (C=O ester), 1694 (C=O aldehyde), 1585 cm^{-1} (C=C py); FAB MS: m/z (%): 166 (100) $[M+H]^+$.

1,2-[{6-(Methoxycarbonyl)pyridin-2-yl}methyleneamino]ethane (2): A solution of ethylenediamine (0.1 mL, 1.51 mmol) in MeOH (10 mL) was added dropwise to a refluxing solution of **1** (0.5 g, 3.010 mmol) in MeOH (30 mL). The resulting mixture was refluxed for 30 min and then filtered while hot. The solvent was removed in a rotary evaporator and diethyl ether (10 mL) was added. The solid formed was isolated by filtration and dried under a vacuum to give 0.40 g (80 %) of **2** as a white powder. ^{1}H NMR (200 MHz, $CDCl_3$, 25 °C, TMS): $\delta=8.55$ (s, 2H; CH=N), 8.21 (dd, $^3J(H,H)=7.3$ Hz, $^4J(H,H)=1.0$ Hz, 2H; py), 8.15 (dd, $^3J(H,H)=8.3$ Hz, $^4J(H,H)=1.0$ Hz, 2H; py), 7.89 (t, 2H; py), 4.07 (s, 4H; -CH_2-), 4.03 ppm (s, 6H; -OCH_3); ^{13}C NMR (50.4 MHz, $CDCl_3$, 25 °C, TMS): $\delta=53.0$ (primary C), 61.1 (secondary C), 162.9, 137.5, 126.2, 124.3 (tertiary C), 165.4, 154.7, 147.6 ppm (quaternary C); elemental analysis calcd (%) for $C_{18}H_{18}N_4O_4$ (354.4): C 61.0, H 5.1, N 15.8; found: C 61.1, H 5.0, N 15.8; IR (KBr): $\tilde{\nu}=1719$ (C=O), 1654 (C=N imine), 1586 cm^{-1} (C=C py); FAB MS: m/z (%): 355 (42) $[M+H]^+$.

1,2-[{6-(Methoxycarbonyl)pyridin-2-yl}methylamino]ethane (3): $NaBH_4$ (0.124 g, 3.30 mmol) was added to a stirred suspension of **2** (0.897 g, 2.53 mmol) in MeOH (60 mL) at 0 °C. The mixture was stirred at 0 °C for 2 h and then a saturated $NaHCO_3$ aqueous solution (200 mL) was added. The mixture was stirred for 10 min, and the resulting solution was extracted with CH_2Cl_2 (5×100 mL). The combined organic extracts were dried over $MgSO_4$ and evaporated to give 0.776 g (85 %) of **3** as a pale yellow oil. ^{1}H NMR (200 MHz, $CDCl_3$, 25 °C, TMS): $\delta=8.01$ (d, $^3J(H,H)=7.8$ Hz, 2H; py), 7.81 (t, $^3J(H,H)=7.8$ Hz, 2H; py), 7.61 (d, $^3J(H,H)=7.8$ Hz, 2H; py), 4.03 (s, 4H; -CH_2-), 3.99 (s, 6H; -OCH_3,), 2.83 ppm (s, 4H; -CH_2-); ^{13}C NMR (50.4 MHz, $CDCl_3$, 25 °C, TMS): $\delta=$ 52.9 (primary C), 49.0, 55.1 (secondary C), 123.5, 125.6, 137.4 (tertiary C), 165.4, 160.8, 165.8 ppm (quaternary C); IR (Nujol): $\tilde{\nu}=1731$ (C=O), 1592 cm^{-1} (C=C py); FAB MS: m/z (%): 359 (75) $[M+H]^+$.

1,2-[*N,N'*-{(*tert*-Butoxycarbonyl)methyl}-*N,N'*-{6-(methoxycarbonyl)pyridin-2-yl}methylamino]ethane (4): The oil **3** (1.60 g, 4.69 mmol) was dissolved in CH_3CN (150 mL) and Na_2CO_3 (1.0 g, 9.4 mmol) and *tert*-butyl-bromoacetate (2 mL, 0.01 mol) were added. The mixture was refluxed under an inert atmosphere (Ar) for 24 h, and then the excess Na_2CO_3 was filtered off. The filtrate was evaporated to dryness and the residue partitioned between equal volumes (100 mL) of H_2O and $CHCl_3$. The organic phase was separated and the aqueous phase washed with more $CHCl_3$ (3×100 mL). The combined organic phases were dried over $MgSO_4$, filtered, and evaporated to dryness to give a pale yellow oil. The crude residue was purified by column chromatography (SiO_2, 5 % MeOH in CH_2Cl_2) to give a pale yellow oil. Addition of diethyl ether gave 0.71 g (26 %) of **4** as a white solid. ^{1}H NMR (200 MHz, $CDCl_3$, 25 °C, TMS): $\delta=7.98$ (d, 2H; py), 7.79 (m, 4H; py), 3.99 (s, 10H; -OCH_3, -CH_2-), 3.31 (s, 4H; -CH_2-), 2.81 (s, 4H; -CH_2-), 1.40 ppm (s, 18H; *t*Bu); ^{13}C NMR (50.4 MHz, $CDCl_3$, 25 °C, TMS): $\delta=28.1$, 52.8 (primary C), 52.5, 56.4, 60.6 (secondary C), 123.5, 126.1, 137.3 (tertiary C), 170.5, 165.9, 160.9, 147.2 ppm (quaternary C); elemental analysis calcd (%) for $C_{30}H_{42}N_4O_8\cdot H_2O$ (604.7): C 59.6, H 7.3, N 9.3; found: C 59.6, H 6.9, N 9.0; IR (KBr): $\tilde{\nu}=1730$, 1710 (C=O), 1587 cm^{-1} (C=C py); FAB MS: m/z (%): 587 (100) $[M+H]^+$.

***N,N'*-Bis(6-carboxy-2-pyridylmethyl)ethylenediamine-*N,N'*-diacetic acid ($H_4L\cdot4HCl\cdot3H_2O$)**: A solution of compound **4** (0.30 g, 0.51 mmol) in 6 M HCl (25 mL) was heated to reflux for 12 h. The solution was concentrated under vacuo to ≈5 mL; this resulted in the precipitation of a white solid. It was collected by filtration and dried under vacuo at 45 °C to yield 0.267 g (81 %) of $H_4L\cdot4HCl\cdot3H_2O$ as a white solid. ^{1}H NMR (200 MHz, D_2O, 25 °C, TMS, pD = 7.0): $\delta=7.82$ (m, 4H; py), 7.51 (d, 2H; py), 4.17 (s, 4H; -CH_2-), 3.91 (s, 4H; -CH_2-), 3.19 ppm (s, 4H; -CH_2-); ^{13}C NMR (50.4 MHz, D_2O, 25 °C, TMS, pD = 7.0): $\delta=51.4$, 57.8, 60.2 (secondary C), 124.3, 127.1, 139.9 (tertiary C), 154.4, 154.7, 173.8, 176.0 ppm (quaternary C); elemental analysis calcd (%) for $C_{20}H_{22}N_4O_8\cdot4HCl\cdot3H_2O$ (586.3): C 37.3, H 5.0, N 8.7; found: C 37.5, H 4.9, N 8.6; IR (KBr): $\tilde{\nu}=$ 1725 (C=O), 1636 cm^{-1} (C=C py); FAB MS: m/z (%): 447 (50) $[M+H]^+$.

Computational methods: Full geometry optimizations of the $[Ln(L)(H_2O)]^-$ systems (Ln = La, Pr, or Gd) were performed at the RHF level both in vacuo and in aqueous solution. In these calculations, the effective core potential (ECP) of Dolg et al. and the related [5s4p3d]-GTO valence basis set were used for the lanthanide atoms,[36] while the 3-21G* basis set was used for the ligand atoms. The calculated stationary points in vacuo were characterized by frequency analysis. Solvent effects were evaluated with the polarizable continuum model (PCM). In particular, we used the C-PCM variant,[55] employing conductor rather than dielectric boundary conditions; this allowed a more robust implementation. The solute cavity was built as an envelope of spheres centered on atoms or atomic groups with appropriate radii. For lanthanide atoms, the previously parametrized radii were used.[37] The cavitation and dispersion non-electrostatic contributions to the energy and energy gradient were omitted. The NMR shielding tensors of $[Ln(L)(H_2O)]^-$ (GIAO[56] method) were calculated both in vacuo and in solution at the at the HF and DFT (B3LYP functional)[57,58] levels with the ECP of Stevens et al.[44] and the 6-311G** basis set for the ligand atoms.[59] For chemical shift calculation purposes, NMR shielding tensors of tetramethylsilane (TMS) were calculated at the appropriate level. All HF and DFT calculations were performed with the Gaussian 98 package (Revision A.11.3).[60]

Analysis of the ^{17}O NMR and NMRD data: Experimental variable-temperature ^{17}O NMR and NMRD data were fit with a computer program written by É. Tóth and L. Helm (Swiss Federal Institute of Technology Lausanne, Switzerland) and a Micromath Scientist version 2.0 (Salt Lake City, UT, USA).

Acknowledgement

M.M.-I. C.P.-I., A.d.B., and T.R.-B. thank the Ministerio de Ciencia y Tecnología and FEDER for financial support (BQU2001–0796). The authors gratefully thank Dr. J.-C. Rodríguez-Ubis (Universidad Autónoma de Madrid, Spain) for recording some of the emission spectra and lifetimes. The authors are indebted to Centro de Supercomputación de Galicia (CESGA) for providing the computer facilities. Likewise, the support and sponsorship provided by COST Action D18 "Lanthanide Chemistry for Diagnosis and Therapy" are kindly acknowledged.

[1] J.-C. G. Bünzli in *Rare Earths* (Eds.: R. Saez-Puche, P. Caro), Editorial Complutense, Madrid, **1998**, p. 223.
[2] *The Chemistry of Contrast Agents in Medical Magnetic Resonance Imaging* (Eds.: A. E. Mebach, É. Tóth), Wiley, New York, **2001**.
[3] P. Caravan, J. J. Ellinson, T. J. McMurry, R. B. Lauffer, *Chem. Rev.* **1999**, *99*, 2293–2352.
[4] P. Hurst, B. K. Takasaki, J. Chin, *J. Am. Chem. Soc.* **1996**, *118*, 9982–9983.
[5] D. Parker, *Coord. Chem. Rev.* **2000**, *205*, 109–130.

[6] M. J. Heeg, S. S. Jurisson, *Acc. Chem. Res.* **1999**, *32*, 1053–1060.
[7] J. A. Peters, J. Huskens, D. J. Raber, *Prog. Nucl. Magn. Reson. Spectrosc.* **1996**, *28*, 283–350.
[8] P. Rongved, T. H. Fritzell, P. Strande, J. Klaveness, *Carbohydr. Res.* **1996**, *287*, 77–89.
[9] D. M. Corsi, L. Vander Elst, R. N. Muller, H. van Bekkum, J. A. Peters, *Chem. Eur. J.* **2001**, *7*, 64–71.
[10] N. Fatin-Rouge, É. Tóth, D. Perret, R. H. Backer, A. E. Merbach, J.-C. G. Bünzli, *J. Am. Chem. Soc.* **2000**, *122*, 10810–10820.
[11] J. P. André, É. Tóth, H. Fisher, A. Seelig, H. R. Mäcke, A. E. Merbach, *Chem. Eur. J.* **1999**, *5*, 2977–2983.
[12] S. Aime, M. Botta, M. Fasano, S. Geminatti Crich, E. Terreno, *Coord. Chem. Rev.* **1999**, *185/186*, 321–333.
[13] S. Aime, E. Gianolio, E. Terreno, G. B. Giovenzana, R. Pagliarin, M. Sisti, G. Palmisano, M. Botta, M. P. Lowe, D. Parker, *J. Biol. Inorg. Chem.* **2000**, *5*, 488–497.
[14] P. Caravan, N. J. Cloutier, M. T. Greenfield, S. A. McDermid, S. U. Dunham, J. W. M. Bulte, J. C. Amedio, Jr., R. J. Looby, R. M. Supkowski, W. DeW. Horrocks, Jr., T. J. McMurry, R. B. Lauffer, *J. Am. Chem. Soc.* **2002**, *124*, 3152–3162.
[15] S. Aime, W. Dastrû, S. Geminatti Crich, E. Gianolio, V. Mainero, *Biopolymers* **2003**, *66*, 419–428.
[16] H. Takalo, I. Hemmila, T. Sutela, M. Latva, *Helv. Chim. Acta* **1996**, *79*, 789–802.
[17] H. Mikola, H. Takalo, I. Hemmila, *Bioconjugate Chem.* **1995**, *6*, 235–241.
[18] S. Achilefu, R. R. Wilhelm, H. N. Jimenez, M. A. Schmidt, A. Srinivasan, *J. Org. Chem.* **2000**, *65*, 1562–1565.
[19] L. Valencia, J. Martínez, A. Macías, R. Bastida, R. A. Carbalho, C. F. G. C. Geraldes, *Inorg. Chem.* **2002**, *41*, 5300–5312.
[20] R. K. Harris, *Nuclear Magnetic Resonance Spectroscopy: A Physicochemical view*, Pitman, London, **1983**.
[21] C. F. G. C. Geraldes, A. M. Urbano, M. A. Hoefnagel, J. A. Peters, *Inorg. Chem.* **1993**, *32*, 2426–2432.
[22] C. Platas-Iglesias, D. M. Corsi, L. Vander Elst, R. N. Muller, D. Imbert, J.-C. G. Bünzli, É. Tóth, T. Maschmeyer, J. A. Peters, *J. Chem. Soc. Dalton Trans.* **2003**, 727–737.
[23] C. Platas, F. Avecilla, A. de Blas, C. F. G. C. Geraldes, T. Rodríguez-Blas, H. Adams, J. Mahía, *Inorg. Chem.* **1999**, *38*, 3190–3199.
[24] B. Bleaney, *J. Magn. Reson.* **1972**, *8*, 91–100.
[25] C. N. Reilley, B. W. Good, J. F. Desreux, *Anal. Chem.* **1975**, *47*, 2110–2116.
[26] R. M. Golding, M. P. Halton, *Aust. J. Chem.* **1972**, *25*, 2577–2581.
[27] A. A. Pinkerton, M. Rossier, S. Stavros, *J. Magn. Reson.* **1985**, *64*, 420–425.
[28] R. E. Davis, M. R. Willcott, *J. Am. Chem. Soc.* **1972**, *94*, 1744–1745.
[29] C. Platas Iglesias, M. Elhabiri, M. Hollenstein, J.-C. Bünzli, C. Piguet, *J. Chem. Soc. Dalton Trans.* **2000**, 2031–2043.
[30] F. Renaud, C. Piguet, G. Bernardelli, J.-C. G. Bünzli, G. Hopfgartner, *Chem. Eur. J.* **1997**, *3*, 1646–1659.
[31] F. J. Steemers, W. Verboom, D. N. Reinhoudt, E. B. Vandertol, J. W. Verhoeven, *J. Am. Chem. Soc.* **1995**, *117*, 9408–9414.
[32] M. Latva, H. Takalo, V. M. Mukkala, C. Matachescu, J.-C. Rodriguez-Ubis, J. Kankare, *J. Lumin.* **1997**, *75*, 149–169.
[33] W. D. Horrocks, Jr., D. R. Sudnick, *J. Am. Chem. Soc.* **1979**, *101*, 334–340.
[34] A. Beeby, I. M. Clarkson, R. S. Dickins, S. Faulkner, D. Parker, L. Royle, A. S. de Sousa, J. A. G. Williams, M. Woods, *J. Chem. Soc. Perkin Trans. 2* **1999**, 493–504.
[35] R. M. Supkowski, W. D. Horrocks, Jr., *Inorg. Chim. Acta* **2002**, *340*, 44–48.
[36] M. Dolg, H. Stoll, A. Savin, H. Preuss, *Theor. Chim. Acta* **1989**, *75*, 173–194.
[37] U. Cosentino, A. Villa, D. Pitea, G. Moro, V. Barone, *J. Phys. Chem. B* **2000**, *104*, 8001–8007.
[38] U. Cosentino, G. Moro, D. Pitea, A. Villa, P. C. Fantucci, A. Maiocchi, F. Uggeri, *J. Phys. Chem. A* **1998**, *102*, 4606–4614.
[39] U. Cosentino, A. Villa, D. Pitea, , G. Moro, V. Barone, A. Maiocchi, *J. Am. Chem. Soc.* **2002**, *124*, 4901–4909.
[40] N. Ouali, B. Bocquet, S. Rigault, P.-Y. Morgantini, J. Weber, C. Piguet, *Inorg. Chem.* **2002**, *41*, 1436–1445.
[41] V. Alexander, *Chem. Rev.* **1995**, *95*, 273–342.
[42] Y. Bretonnière, M. Mazzanti, J. Pécaut, F. A. Dunand, A. E. Merbach, *Inorg. Chem.* **2001**, *40*, 6737–6745.
[43] P. Caravan, A. V. Astashkin, A. M. Raitsimring, *Inorg. Chem.* **2003**, *42*, 3972–3974.
[44] W. J. Stevens, M. Krauss, H. Basch, P. G. Jasien, *Can. J. Chem.* **1992**, *70*, 612–630.
[45] J. H. Forsberg, R. M. Delaney, Q. Zhao, G. Harakas, R. Chandran, *Inorg. Chem.* **1995**, *34*, 3705–3715.
[46] J. Lisowski, J. L. Sessler, V. Lynch, T. D. Mody, *J. Am. Chem. Soc.* **1995**, *117*, 2273–2285.
[47] J. Reuben, D. Fiat, *J. Chem. Phys.* **1969**, *51*, 4918–4927.
[48] M. Gueron, *J. Magn. Reson.* **1975**, *19*, 58–66.
[49] A. J. Vega, D. Fiat, *Mol. Phys.* **1976**, *31*, 347–355.
[50] D. H. Powell, O. M. Ni Dhubhghaill, D. Pubanz, L. Helm, Y. S. Lebedev, W. Schlaepfer, A. E. Merbach, *J. Am. Chem. Soc.* **1996**, *118*, 9333–9346.
[51] E. J. T. Chrystal, L. Couper, D. J. Robins, *Tetrahedron* **1995**, *51*, 10241–10252.
[52] S. R. Meech, D. J. Philips, *J. Photochem.* **1983**, *23*, 193–217.
[53] R. L. Vold, J. S. Waugh, M. P. Klein, D. E. Phelps, *J. Chem. Phys.* **1968**, *48*, 3831–3832.
[54] S. Meiboom, D. Gill, *Rev. Sci. Instrum.* **1958**, *29*, 688–691.
[55] V. Barone, M. Cossi, *J. Phys. Chem. A* **1998**, *102*, 1995–2001.
[56] R. Ditchfield, *Mol. Phys.* **1974**, *27*, 789–807.
[57] A. D. Becke, *J. Chem. Phys.* **1993**, *98*, 5648–5652.
[58] C. Lee, W. Yang, R. G. Parr, *Phys. Rev. B* **1988**, *37*, 785–789.
[59] A description of the basis sets and theory level used in this work can be found in J. B. Foresman, A. E. Frisch, *Exploring Chemistry with Electronic Structure Methods*, 2nd ed., Gaussian Inc., Pittsburgh, PA, **1996**.
[60] Gaussian 98 (Revision A.7), M. J. Frisch, G. W. Trucks, H. B. Schlegel, G. E. Scuseria, M. A. Robb, J. R. Cheeseman, V. G. Zakrzewski, J. A. Montgomery, Jr., R. E. Stratmann, J. C. Burant, S. Dapprich, J. M. Millam, A. D. Daniels, K. N. Kudin, M. C. Strain, O. Farkas, J. Tomasi, V. Barone, M. Cossi, R. Cammi, B. Mennucci, C. Pomelli, C. Adamo, S. Clifford, J. Ochterski, G. A. Petersson, P. Y. Ayala, Q. Cui, K. Morokuma, D. K. Malick, A. D. Rabuck, K. Raghavachari, J. B. Foresman, J. Cioslowski, J. V. Ortiz, B. B. Stefanov, G. Liu, A. Liashenko, P. Piskorz, I. Komaromi, R. Gomperts, R. L. Martin, D. J. Fox, T. Keith, M. A. Al-Laham, C. Y. Peng, A. Nanayakkara, C. Gonzalez, M. Challacombe, P. M. W. Gill, B. G. Johnson, W. Chen, M. W. Wong, J. L. Andres, M. Head-Gordon, E. S. Replogle, J. A. Pople, Gaussian, Inc., Pittsburgh, PA, **1998**.

Received: December 17, 2003
Revised: February 26, 2004
Published online: June 3, 2004

